Biophysical Chemistry 149 (2010) 22–27

Contents lists available at ScienceDirect

Biophysical Chemistry

journal homepage: http://www.elsevier.com/locate/biophyschem

Flexible loops of thread-like micelles are formed upon interaction of L-α-dimyristoyl-phosphatidylcholine with the biosurfactant surfactin as revealed by cryo-electron tomography

Christoph Boettcher [a,*], Henny Kell [b], Josef F. Holzwarth [c], Joachim Vater [b]

[a] Forschungszentrum für Elektronenmikroskopie, Institut für Chemie und Biochemie, Freie Universität Berlin, Fabeckstr. 36a, D-14195 Berlin, Germany
[b] Institut für Chemie, Arbeitsgruppe Biochemie und Molekulare Biologie, Technische Universität Berlin, Franklinstr. 29, D-10587 Berlin, Germany
[c] Fritz-Haber-Institut, Max-Planck-Society, Faradayweg 4-6, 14195 Berlin, Germany

ARTICLE INFO

Article history:
Received 13 January 2010
Received in revised form 8 March 2010
Accepted 10 March 2010
Available online 16 March 2010

Keywords:
Surfactin
Mixed DMPC–surfactin-micelles
Cryo-electron microscopy
Cryo-electron tomography

ABSTRACT

Vesicles of L-α-dimyristoyl-phosphatidylcholine (DMPC) are known to disintegrate upon treatment with surfactin, a lipoheptapeptide biosurfactant from *Bacillus subtilis* OKB 105, as was observed by static light scattering (SLS) and cryo-transmission electron microscopy (cryo-TEM) recently. The lysis of DMPC bilayers occurs strongly dependent on the surfactin concentration according to a three-stage model. Unilamellar DMPC vesicles are disrupted to form sheet-like lamellar intermediates at a moderate surfactant concentration, but undergo a transition towards smaller particles of unknown structure at a higher surfactant concentration according to earlier neutron scattering experiments. Here we present direct structural evidence from cryo-electron tomography data that thread-like micelles with a uniform diameter of 6.5 nm are organized into loops of different sizes at a surfactin concentration of >15 mol%.

1. Introduction

Biosurfactants are a subject of intense research, because of their prospect for unique biotechnological and medical applications [1–5]. Of particular attraction are the surfactins, a family of cyclic lipoheptapeptides which are produced by numerous *Bacillus subtilis* [6,7] and *B. amyloliquefaciens* strains [8]. They are composed of a heptapeptide linked to a β-hydroxy fatty acid with chain lengths of 12–15 carbon atoms cyclized by macrolactone formation [9–11] as shown in the scheme. Natural surfactin is a complex of isoforms due to variations of fatty acid branching and chain length [6,12] as well as amino acid substitutions in the peptide ring [7,13] (Scheme 1 [9–12]).

Surfactins belong to the most potent biosurfactants [1,2], which is reflected in their antimicrobial [1,14], antiviral [15,16], antimycoplasmatic [17] and hemolytic activities [14,18]. Of particular relevance are their degrading effects on lipid-enveloped viruses [15,16] and mycoplasma [17] which explains the high medical and biotechnological interest. Surfactin is e.g. already commercially used as a potent antimycoplasma agent for curing cell cultures and biotechnological products from mycoplasma contamination. Its utilisation as an antiviral agent is under current development.

Due to their specific amphiphilic structure surfactins show unique surface-, interface- and membrane-active properties by integrating into lipid vesicles [19,20] or monolayers [21–25] and they possess a high tendency for self-aggregation by forming micelles [26–29]. Previous studies on the effects of surfactin on mycoplasma and membrane coated viruses [16,17] revealed a pure physicochemical mechanism which leads to the disintegration of the envelop lipid membranes. The mode of surfactin activity was visualized by thin sectioning electron microscopy of mycoplasma in cultures of contaminated mammalian cells [17]. At micromolar concentrations of surfactin the mycoplasma cells begin to swell due to permeability changes induced by the biosurfactant. At a surfactin concentration above the CMC mycoplasma species were completely disrupted by fragmentation of their membrane envelope.

The clue for understanding the biological activity of surfactin is to directly study its impact on the structure of biological membranes. To investigate its mechanism of action on the molecular level and to design efficient procedures for biotechnological usage biomimetic studies of surfactin interaction with model membranes are needed. With this aim we recently initiated systematic examinations of surfactin's lytic action on unilamellar DMPC vesicles using physicochemical techniques such as differential scanning calorimetry (DSC), static light scattering (SLS), small angle neutron scattering (SANS) and cryo-electron microscopy (cryo-TEM) [20].

The disintegration of DMPC vesicles by surfactin was observed to be consistent with a three-stage model described earlier for lipid bilayer dissolution by conventional nonionic and ionic synthetic surfactants [30,31]. In analogy, surfactin is integrated into the lipid bilayer without detectable structural changes of the membrane at a low surfactant concentration of <4 mol% (stage one). In the second

* Corresponding author. Tel.: +49 30 838543934; fax: +49 30 83856589.
E-mail address: christoph.boettcher@fzem.fu-berlin.de (C. Boettcher).

0301-4622/$ – see front matter © 2010 Elsevier B.V. All rights reserved.
doi:10.1016/j.bpc.2010.03.006

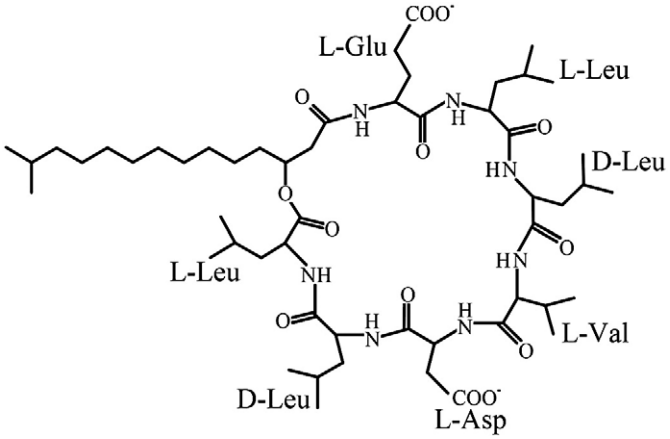

Scheme 1. Structural formula of surfactin.

stage the lipid bilayer is progressively disrupted due to increasing strains in the membrane by further uptake of surfactin molecules leading to the formation of sheet-like, lamellar particles visible by cryo-electron microscopy. Ultimately, in the third stage above 15 mol% of surfactin ellipsoidal particles were detected by small angle neutron scattering thought to correspond to phospholipid-surfactin mixed micelles. They have not yet been visualized by direct imaging methods and thus the structural aspects remained only hypothetical so far.

In this paper we report on the direct structural characterization of these particles by cryo-TEM measurements. The images unveiled manifold structural species which had the appearance of rings, linear as well as branched fibers and densely entangled fiber networks (Fig. 2B). In order to fully understand the structural organisation of these aggregates in three dimensions we performed tomographic series of the vitrified sample layer where individual micellar asssemblies can be viewed in different spatial orientations. Comparing these data with cryo-TEM images of pure surfactin solutions, which showed exclusively small spherical or slightly elongated micelles, it became evident that the interaction of surfactin with DMPC vesicles at a surfactin concentration of more than 15 mol% promotes the formation of supramolecular aggregates, which are very different from the vesicular organisation of the pure DMPC solution.

2. Materials and methods

2.1. Materials

Surfactin was produced by fermentation of the recombinant high producer strain *B. subtilis* OKB 105, as reported by Baumgart et al. [32]. L-α-dimyristoyl phosphatidyl-choline (DMPC) was obtained from Sigma-Aldrich (Taufkirchen, Germany). DMPC vesicles were prepared, as described in a previous publication [20].

0.5 ml of a 36 mM ethanolic DMPC solution were slowly added over a period of one hour into 10 ml 2.5 mM Tricine-buffer at pH 7.5 by injection with a Hamilton syringe. During the preparation the temperature of the solution was kept at 30 °C, which is above the lipid's phase transition temperature (T_{MPT} = 23.5 °C) to achieve the formation of the fluid state. Thereafter ethanol was removed by dialysis against 2.5 mM Tricine–HCl buffer at 30 °C for at least 16 h. The solution remains stable for several days, if kept at 30 °C. The stability of the vesicles was tested by measuring the solution turbidity.

DMPC/surfactin samples were prepared by mixing the appropriate volume of a 10 mM stock solution of surfactin in methanol with the dialyzed DMPC solution above the phase transition temperature. For cryogenic transmission electron microscopy (cryo-TEM) the samples contained 2.5 mM DMPC and 0.75 mM surfactin (30 mol%). The methanol concentration in the reaction mixture was 3% (v/v) which showed no effect on the morphology of the DMPC vesicles, as controlled by cryo-TEM.

2.2. Cryogenic transmission electron microscopy (cryo-TEM)

The samples for cryogenic transmission electron microscopy (cryo-TEM) were prepared at an ambient temperature of 30 °C and saturated humidity in a custom-made CEVS apparatus ("controlled environment vitrification system") according to Talmon et al. [33]. Under these temperature and humidity controlled conditions a droplet (6 μl) of the solution was placed on hydrophilized (60 s plasma treatment at 8 W using a BALTEC MED 020 device), perforated carbon filmed *Quantifoil* grids (R1/4 batch of Quantifoil Micro Tools GmbH, Jena, Germany). The excess fluid was blotted off to create an ultra thin layer (typical thickness of 100–200 nm) of the solution spanning the holes of the carbon film. The grids were immediately vitrified by propelling the grid through a shutter of the CEVS into a vessel placed right below the shutter containing liquid ethane at its freezing point (−184 °C). Ultra-fast cooling is necessary for an artifact-free thermal fixation ("vitrification") of the aqueous solution avoiding crystallization of the solvent or rearrangement of the assemblies. The vitrified samples were transferred under liquid nitrogen into a Philips Tecnai F20 transmission electron microscope (FEI company, Oregon, USA) using the Gatan (Gatan Inc., California, USA) cryoholder and -stage (Model 626). Microscopy was carried out at −175 °C sample temperature using the microscope's low-dose mode at a calibrated primary magnification of 62,000×. Images were recorded using a 2 k-Eagle CCD camera at full resolution (2048 × 2048 pixel). The accelerating voltage was 160 kV and the defocus was chosen to be 2 μm.

2.3. Cryogenic electron tomography (cryo-ET)

Sample preparation for tomography was performed in the same way as for conventional cryo-TEM described above. The vitrified grids were transferred by the use of a Gatan tomography cryoholder (Model CT3500) into a Tecnai F20 transmission electron microscope equipped with a field emission gun operating at 160 kV. Images were recorded using a 2 k-Eagle CCD camera at full resolution (2048 × 2048 pixel). Tilt series were recorded under low-dose conditions collecting images between −22.5° and +22.5° (45° segment) in 1° tilt increments accumulating a total electron dose of $<100\ eÅ^{-2}$. The primary magnification was 25 k corresponding to a pixel size of 1.12 nm in the images. The defocus was chosen at a high value of 10 μm in order to create sufficient phase contrast in the images of the relatively low-contrast aggregates. The three-dimensional reconstruction based on the tomographic series was determined by the use of the Inspect 3D software (FEI company, Oregon, USA) by employing the SIRT projection algorithm. Corresponding projection images into the reconstructed volume (Fig. 2B) were calculated by means of IMAGIC V (Image Science GmbH, Berlin, Germany) image processing software. 3D-model data were generated by the use of AMIRA software V5.0 (Visage Imaging GmbH, Berlin, Germany).

3. Results and discussion

In order to better understand the very effective biological activity of the lipoheptapeptide surfactin on microorganisms and enveloped viruses which is of notable medical and biotechnological potentials we perform biomimetic studies on the surfactin interaction with artifical lipid membranes. In a previous paper we started [20] to investigate the disintegration of unilamellar DMPC vesicles at different surfactin concentrations. We detected three forms of DMPC–surfactin-aggregates by differential scanning calorimetry (DSC) and static light

scattering (SLS). A structural characterization was complemented by cryo-electron microscopy (cryo-TEM) and small angle neutron scattering (SANS). Here we complete these studies by analysing the final putatively micellar product (indicated by neutron scattering data) in three dimensions by using the cryo-electron tomography technique. The solubilisation of DMPC vesicles by surfactin showed a typical three-stage sequence. In stage one at low surfactin concentration up to ~4 mol% cryo-TEM showed typical vesicles which were progressively converted into sheet-like lamellar fragments upon the increase of the surfactin concentration in the range of 4–15 mol% (stage two).

Above 15 mol% of surfactin a third form of DMPC–surfactin aggregates was formed in an irreversible process as indicated by SANS measurements [20]. The data point to the formation of ellipsoidal particles corresponding to DMPC–surfactin mixed micelles (stage three). The aim of this paper was now the direct visualization and structural characterization of this third form of DMPC–surfactin aggregates by the use of cryo-TEM. However, the complexity of the obtained image data (see below) required additional tomographic image series in order to understand the spatial organisation of the assemblies. With this obtained information at hand the third species of mixed DMPC–surfactin micelles can now be fully described in three dimensions.

In a first control experiment by cryo-TEM we characterized the aggregation behaviour of pure surfactin in the concentration range (30 mol%) used for the later experiments with DMPC which is well above the surfactant's cmc. Pure surfactin at 30 mol% (0.75 mM) showed a monodisperse distribution of small spherical or slightly ellipsoidal micelles with a diameter of ~4–5 nm as is shown in Fig. 1a. This finding fully coincides with earlier TEM data reported by Knoblich et al. [27].

Fig. 1b shows a typical cryo-TEM micrograph of the DMPC–surfactin mixture at a surfactin concentration of 30 mol%. At first sight the micrographs descriptively comprise structural features such as ring-, rod- and network-like assemblies (denoted in Fig. 1b). Interestingly, the diameter of all the aggregates underlying elemental motif which resembles a thread-like geometry is identical and amounts to approximately 6.5 nm.

However, at this stage of data observation it appeared quite difficult to fully understand the underlying spatial arrangement of the assemblies as they appeared structurally very different. In particular, the coexistence of high contrast rods and rings of lower contrast had to be clarified. Even more, the relation to the frequently observed networks was not clear. We therefore employed cryo-ET of the vitrified sample to learn about the structural differences at various spatial orientations. However, the radiation sensitivity of the frozen sample limits the number of images which can be recorded of an individual sample location. Consequently, the included angle for imaging was limited to only 45°. Fortunately, this small angular segment allows to fully describe the three-dimensional organisation of the structural features shown in Fig. 1b. For a straightforward discussion we present three selected images from a three-dimensional volume reconstruction (calculated from the tomographic series) as projection images at different view angles that are +18°, 0° and −18° (Fig. 2 and Supplementary Multimedia Video File). The tomographic approach provides the advantage over simple tilt-pair imaging that individual view angles of the objects can be chosen from the data where superposition with neighbouring assemblies are absent.

Arrows in Fig. 2 indicate the view-angle dependent projection images of selected aggregates. It becomes evident that in those cases where obvious ring-like structures become orientated with their "thread-surface" upright the projection images provide a rod-like appearance upon tilting. Changes of the density within the aggregate upon tilting fully agree with the projection images of a ring-like ultrastructure and even allow to observe the cross section of its constituting cylindrical micelle with a circular diameter of 6.5 nm (e.g. Fig. 1b, dotted line arrow at 18°). Moreover, the data allow to fully interpret all other structural features present in the image. We now understand that the majority of assemblies are organized as loops with varying diameters between 10 and 60 nm. As the diameter of the loops increases, the flexibility appears to increase similarly, i.e. some of the larger loops show a high tendency for bending or even possess kinks. Such deviations from the planar geometry explain the multiplicity of structural entities in the images, which become even more complicated by the fact that all densities of a three-dimensional object or cluster of objects accumulate in the microscope's image plane, if the electrons permeate the sample (cp. simulation in Fig. 3).

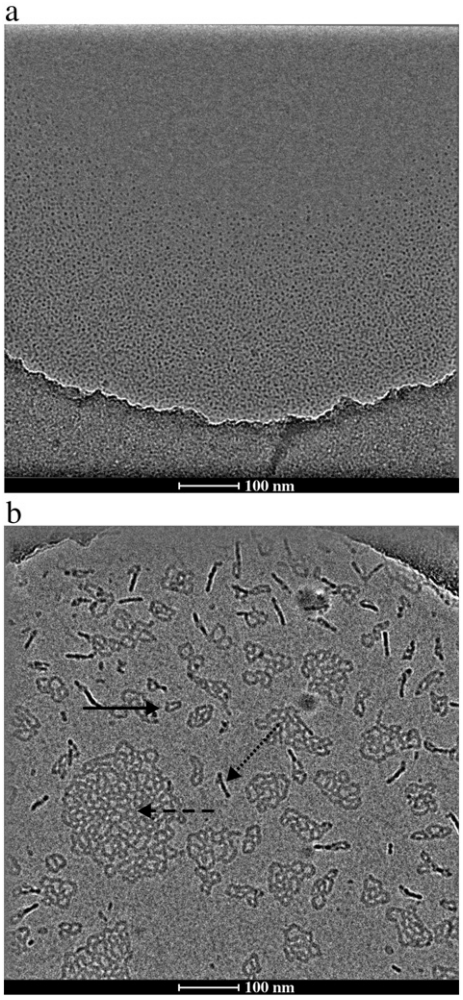

Fig. 1. (a) Cryo-TEM image of pure surfactin micelles at 30 mol% (b) Cryo-TEM image of mixed DMPC–surfactin micelles at a DMPC-concentration of 2.5 mM and a surfactin concentration of 30 mol%. The images were slightly band-pass filtered for better visibility. Different structural features are indicated by arrows: ring-structure (straight arrow), rod-structure (dotted arrow), network assembly (dashed arrow).

In the case of networks we learn from the tomographic data that they just result from a conglomerate of individual micellar loops. The data reveal clearly that most loops are individualized over the 3D volume (the layer thickness is usually between 100 and 200 nm) though they appear to be interconnected in single projection images. However interconnected or branched loops also exist in rare cases (e.g. Fig. 1b, dashed arrows).

The dimension (6.5 nm) and structure of the thread-like micelle, which is the elemental motif for all the assemblies visible in the images, indicates that surfactin must somehow contribute to a new mixed micellar organisation as the structural features are different from pure DMPC or surfactin preparations, respectively. The thread-

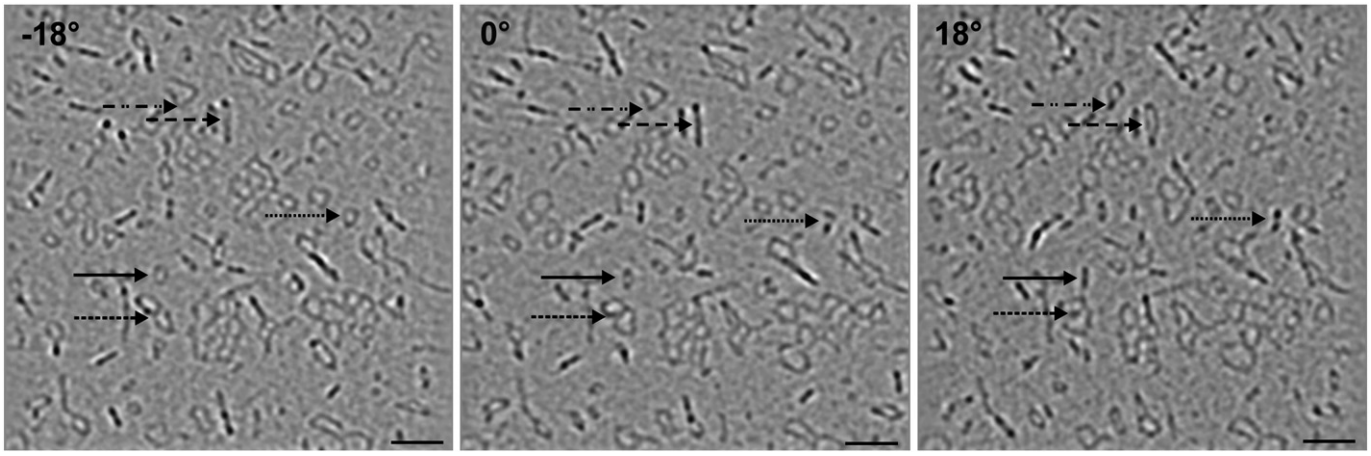

Fig. 2. Cryo-ET data of the DMPC–surfactin mixture as shown in Fig. 1b. Three selected projections (−18°, 0°,+18°) of a reconstructed 3D-volume calculated from a tomographic series in a tilt angle range between −22.5 and +22.5° (1° increment). Straight and dotted arrows depict ring-like micelles which show expected geometrical and density changes upon sample tilting. Note the circular profile of the micellar cylinder at +18°. In addition, larger micellar loops (dashed arrow), which might be branched (small-dashed arrow) or show kinks (dashed-and dotted arrow) built up the network assemblies if they are in close lateral and horizontal spatial proximity (Bar is 100 nm).

like micelles neither show the bilayer profile and the typical 4 nm thickness of the DMPC membrane nor can we find individual spherical micelles of 4 nm diameter which are the common ultrastructural organisation of pure surfactin (Fig. 1a).

The cylindrical mixed micelle do not show a bilayer density profile though it was occasionally found for spherical and fiber-like micellar aggregates [34,35]. Even at carefully chosen imaging conditions at higher magnification and close-to-focus conditions at which a sharp bilayer profile of lipid vesicle membranes is obtained exclusively thread-micelles without density variations are observed (Fig. 1b). This finding indicates that the integration of both lipid as well as surfactant molecules within a mixed micelle creates an ultra-structure which is different from the typical bilayer organisation.

It appears plausible that the extended horse-saddle structure of surfactin [36] has a structural impact on the organisation of the lipid molecules. Here, the wedge-like geometry of surfactin might determine the magnitude of penetration and thus creates a widening of the bilayered geometry of a lipid membrane from 4 nm to 6.5 nm. Interestingly, there are only very rarely loose micelle ends detectable in the preparation. The type of mixed micelles formed here obviously avoids the high energetic micellar end-caps (frequently observed with fiber micelles) by forming closed circular assemblies. Due to the different head group geometries of the participating molecules an out-of-register organisation in a mixed aggregate is comprehensible, which might explain the missing bi-layer density profile.

Fig. 3 shows a computer simulation of loop-like organized cylindrical micelles in a 3D-volume analogous to those detected by cryo-ET. The observation of these assemblies from arbitrarily selected view angles explains the complexity of the TEM data and even more, if projection images are considered, as shown in the lower row of Fig. 3. Due to different superposition with respect of the viewing angle the changes of the structures become intelligible: a planar ring

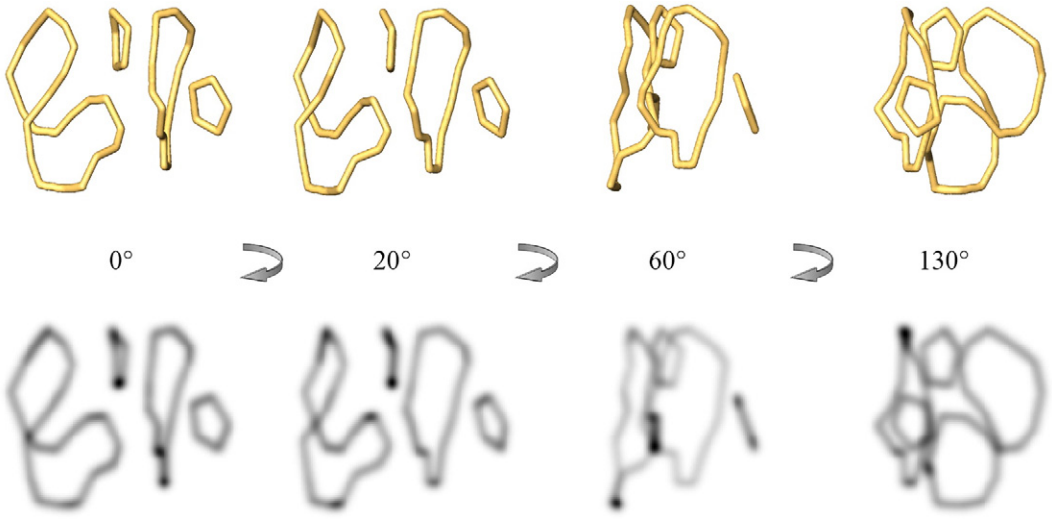

Fig. 3. (Upper row) Computer generated 3D-model of an ensemble of thread-like micelles with different geometry (planar ring, small ring with kink, bent rings of different size) viewed from different directions if rotated around the *z*-axis. The four motifs represent the structural features found for the DMPC/surfactin system in the tomographic reconstruction (Fig. 2). Due to different superposition with respect of the viewing angle the changes of the structures become intelligible: a planar ring converts into a rod in edge-on orientation. A small ring with kink becomes a bent rod. All structures in superposition (cp. 130° view) create the impression of an entangled network. (Lower row) Corresponding projection images of the above 3D-model illustrate the changes in the densities depending on the orientation of the respective motifs. The calculated projection patterns correlate nicely with the microscopical data.

converts into a rod in edge-on orientation. A small ring with kink becomes a bent rod. All structures in superposition (cp. 130° view) create the impression of an entangled network.

The fundamental principle for the disintegration of lipid membranes both by conventional synthetic surfactants and those of biological origin is the three-stage model [30,31]. The mode of action is a theme with variations as far as the intermediates and end products of the disintegration pathways are concerned. The individual changes depend strongly on the original lipid material, the nature of the surfactant and the physicochemical parameters.

The application of cryo-TEM for direct imaging of the morphological transformations on the interaction of lipid membranes with conventional surfactants started about two decades ago [31]. Representative examples were the surfactant induced disintegration of lecithin vesicles [37–41] and sterically stabilized poly(ethylene glycol)-liposomes [42,43]. In particular, the vesicle–micelle transitions of egg phosphatidyl choline by nonionic [37–39] and charged [40,41] surfactants show striking similarities to the sequence of morphological changes observed in our work using DMPC and surfactin. Here, lamellar vesicles are converted into bilayers fragments followed by a transformation into thread-like cylindrical mixed micelles upon increasing surfactant concentration. At the highest surfactant concentrations spheroidal micelles were formed as the end products.

During the last decade great progress has also been achieved with regard to the visualization of lipid–biosurfactant aggregates using advanced TEM- [20,44,45] and AFM- [22–25,46] techniques. For example, similar results have been reported for the interaction of fengycins with phospholipid membranes [45]. Fengycins represent a family of cyclolipodecapeptides produced by numerous *B. subtilis* and *B. amyloliquefaciens* strains [6–8]. Concerning their effects on the morphology of unilamellar DPPC-vesicles also here three different stages could be discerned. At high fengycin concentrations above 30 mol% the bilayers were completely disrupted and entangled thread-like aggregates were visualized by cryo-TEM which were suggested to be mixed micelles of DPPC and fengycin.

4. Conclusions

Our results on the destabilization of phospholipid membranes such as DMPC and DPPC by surfactin are consistent with the reported three-stage model for the disintegration of lipid membranes by surfactants [30,31]. Each phase could be individually characterized by cryo-TEM in combination with differential scanning calorimetry and static light scattering measurements. The process starts from unilamellar, bilayered vesicles (stage one, vesicular phase) which can be saturated with surfactin up to a biosurfactant concentration of 4 mol% without any visible changes of the vesicle ultra-structure. At surfactin concentrations above 4 up to approximately 10 mol% DMPC vesicles disintegrate and transform into sheet-like lamellar fragments (stage two, phase of intermediates). In the final stage, at a surfactin concentrations higher than 10 mol% (stage three, micellar phase), thread-like mixed micelles with a uniform diameter of 6.5 nm were detected which tend to form loop-like aggregates of various size. The flexible nature of the latter and the variations in the size pretended a high structural variety. Tomography however revealed, that the aggregation can be traced back to the formation of a simple micellar motif. However, the exact nature of the mixed organisation of lipid and surfactant in the micelle is still not clear, but must be different from the bilayered in-register arrangement typically found for each system individually.

Acknowledgement

The authors would like to thank Drs. B. Schade and K. Ludwig for help with the model data.

Appendix A. Supplementary data

Supplementary data associated with this article can be found, in the online version, at doi:10.1016/j.bpc.2010.03.006.

References

[1] J. Vater, Lipopeptides, an attractive class of microbial surfactants, Progr. Colloid Polymer Sci. 72 (1986) 12–18.
[2] J.D. Desai, I.M. Banat, Microbial production of surfactants and their commercial potential, Microbiol. Mol. Biol. Rev. 61 (1997) 47–64.
[3] S.S. Cameotra, R.S. Makkar, Recent applications of biosurfactants as biological and immunological molecules, Curr. Opin. Microbiol. 7 (2004) 262–266.
[4] P. Singh, S.S. Cameotra, Potential applications of microbial surfactants in biomedical sciences, Trends Biotechnol. 22 (2004) 142–146.
[5] L. Rodrigues, I.M. Banat, J. Teixeira, R. Oliveira, Biosurfactants: potential applications in medicine, J. Antimicrob. Chemother. 57 (2006) 609–618.
[6] J. Vater, X. Gao, G. Hitzeroth, C. Wilde, P. Franke, "Whole Cell"-matrix-assisted laser desorption ionization-time of flight-mass spectrometry, an emerging technique for efficient screening of biocombinatorial libraries of natural compounds — present state of research, Comb. Chem. High Throughput Screen. 6 (2003) 557–667.
[7] J.-M. Bonmatin, O. Laprevote, F. Peypoux, Diversity among microbial cyclic lipopeptides: iturins and surfactins. Activity–structure relationships to design new bioactive agents, Comb. Chem. High Throughput Screen. 6 (2003) 79–99.
[8] A. Koumoutsi, X.-H. Chen, A. Henke, H. Liesegang, G. Hitzeroth, P. Franke, J. Vater, R. Borriss, Structural and functional characterization of gene clusters directing nonribosomal synthesis of bioactive cyclic lipopeptides in *Bacillus amyloliquefaciens* strain FZB42, J. Bacteriol. 186 (2004) 1084–1096.
[9] A. Kakinuma, M. Hori, M. Isono, G. Tamura, K. Arima, Determination of amino acid sequence in surfactin, a crystalline peptidelipid surfactant produced by *Bacillus subtilis*, Agric. Biol. Chem. 33 (1969) 971–972.
[10] A. Kakinuma, H. Sugino, M. Isono, G. Tamura, K. Arima, Determination of fatty acid in surfactin and elucidation of the structure of surfactin, Agric. Biol. Chem. 33 (1969) 973–976.
[11] A. Kakinuma, M. Hori, H. Sugino, J. Yoshida, M. Isono, G. Tamura, K. Arima, Determination of the location of lactone ring in surfactin, Agric. Biol. Chem. 33 (1969) 1523–1524.
[12] M. Kowall, J. Vater, B. Kluge, T. Stein, P. Franke, D. Ziessow, Separation and characterization of surfactin isoforms produced by *Bacillus subtilis* OKB105, J. Colloid Interface Sci. 204 (1998) 1–8.
[13] F. Peypoux, J.M. Bonmatin, J. Wallach, Recent trends in the biochemistry of surfactin, Appl. Microbiol. Biotechnol. 51 (1999) 553–563.
[14] A.W. Bernheimer, L.S. Avigad, Nature and properties of a cytolytic agent produced by *B. subtilis*, J. Gen. Microbiol. 61 (1970) 361–369.
[15] H. Itokawa, T. Miyashita, H. Morita, K. Takeya, T. Hirano, M. Homma, K. Oka, Structural and conformational studies of [Ile^7] and [Leu^7] surfactins from *Bacillus subtilis* natto, Chem. Pharm. Bull. 42 (1994) 604–607.
[16] D. Vollenbroich, M. Özel, J. Vater, R.M. Kamp, G. Pauli, Mechanism of inactivation of enveloped viruses by the biosurfactant surfactin from *Bacillus subtilis*, Biologicals 25 (1997) 289–297.
[17] D. Vollenbroich, G. Pauli, M. Özel, J. Vater, Antimycoplasma properties and application in cell culture of surfactin, a lipopeptide antibiotic from *Bacillus subtilis*, Appl. Environ. Microbiol. 63 (1997) 44–49.
[18] M. Kracht, H. Rokos, M. Özel, M. Kowall, G. Pauli, J. Vater, Antiviral and hemolytic activities of surfactin isoforms and their methylester derivatives, J. Antibiot. 52 (1999) 613–619.
[19] J.C. Grau, F. Gomez Fernandez, F. Peypoux, A. Ortiz, A study on the interactions of surfactin with phospholipid vesicles, Biochim. Biophys. Acta 1418 (1999) 307–319.
[20] H. Kell, J.F. Holzwarth, C. Böttcher, R.K. Heenan, J. Vater, Physicochemical studies of the interaction of the lipoheptapeptide surfactin with lipid bilayers of L-α-dimyristoyl phosphatidylcholine, Biophys. Chem. 128 (2007) 114–124.
[21] R. Maget-Dana, M. Ptak, Interactions of surfactin with membrane models, Biophys. J. 68 (1995) 1937–1943.
[22] M. Deleu, M. Paquot, P. Jacques, P. Thonart, Y. Adriaensen, Y.F. Dufrene, Nanometer scale organization of mixed surfactin/phosphatidylcholine monolayers, Biophys. J. 77 (1999) 2304–2310.
[23] M. Deleu, K. Knott, R. Brasseur, P. Jacques, P. Thonart, Y.F. Dufrene, Imaging mixed lipid monolayers by dynamic atomic force microscopy, Biochim. Biophys. Acta 1513 (2001) 55–62.
[24] M. Eeman, A. Berquand, Y.F. Dufrene, M. Paquot, S. Dufour, M. Deleu, Penetration of surfactin into phospholipid monolayers: nanoscale interfacial organization, Langmuir 22 (2006) 11337–11345.
[25] O. Bouffioux, A. Berquand, M. Eeman, M. Paquot, Y.F. Dufrene, R. Brasseur, M. Deleu, Molecular organization of surfactin-phospholipid monolayers: effect of phospholipid chain length and polar head, Biochim. Biophys. Acta 1768 (2007) 1758–1768.
[26] Y. Ishigami, M. Osman, H. Nakahara, Y. Sano, R. Ishiguro, M. Matsumoto, Significance of β-sheet formation for micellization and surface adsorption of surfactin, Colloids Surf. B: Biointerfaces 4 (1995) 341–348.
[27] A. Knoblich, M. Matsumoto, R. Ishiguro, K. Murata, Y. Fujiyoshi, Y. Ishigami, M. Osman, Electron cryo-microscopic studies on micellar shape and size of surfactin, an anionic lipopeptide, Colloids Surf. B: Biointerfaces 5 (1995) 43–48.

[28] H. Heerklotz, J. Seelig, Detergent-like action of the antibiotic peptide surfactin on lipid membranes, Biophys. J. 81 (2001) 1547–1554.
[29] P. Tsan, L. Volpon, F. Besson, J.-M. Lancelin, Structure and dynamics of surfactin studied by NMR in micellar media, J. Am. Chem. Soc. 129 (2007) 1968–1977.
[30] J. Lasch, Interaction of detergents with lipid vesicles, Biochim. Biophys. Acta 1241 (1995) 269–292.
[31] M. Almgren, Mixed micelles and other structures in the solubilization of bilayer lipid membranes by surfactants, Biochim. Biophys. Acta 1508 (2000) 146–163.
[32] F. Baumgart, B. Kluge, C. Ullrich, J. Vater, D. Ziessow, Identification of amino acid substitutions in the lipopeptide surfactin using 2D NMR spectroscopy, Biochem. Biophys. Res. Commun. 177 (1991) 998–1005.
[33] J.R. Bellare, H.T. Davis, L.E. Scriven, Y. Talmon, Controlled environment vitrification system (CEVS): An improved sample preparation technique, J. Electron Microsc. Tech. 10 (1988) 87–111.
[34] M. Kellermann, W. Bauer, A. Hirsch, B. Schade, K. Ludwig, C. Böttcher, The first account on a structurally persistent micelle, Angew. Chem. 116 (2004) 3019–3022; Int. Ed. 43 (2004) 2959–2962.
[35] C. Boettcher, H. Stark, M. van Heel, Stacked bilayer helices: a new structural organisation of amphiphilic molecules, Ultramicroscopy 62 (1996) 133–139.
[36] J.-M. Bonmatin, M. Genest, H. Labbé, M. Ptak, Solution three-dimensional structure of surfactin: a cyclic lipopeptide studied by ^{1}H NMR, distance geometry and molecular dynamics, Biopolymers 34 (1994) 975–986.
[37] P.K. Vinson, Y. Talmon, A. Walter, Vesicle–micelle transition of phosphatidylcholine and octyl glucoside elucidated by cryo-transmission electron microscopy, Biophys. J. 56 (1989) 669–681.
[38] K. Edwards, M. Almgren, J. Bellare, W. Brown, Effects of Triton X-100 on sonicated lecithin vesicles, Langmuir 5 (1989) 473–478.
[39] K. Edwards, M. Almgren, Solubilization of lecithin vesicles by $C_{12}E_8$. Structural transitions and temperature effects, Colloid Interf. Sci. 147 (1991) 1–21.
[40] K. Edwards, M. Almgren, J. Gustafsson, G. Karlsson, Solubilization of lecithin vesicles by a cationic surfactant. Intermediate structure in the vesicle–micelle transition observed by cryo-TEM, J. Colloid Interf. Sci. 161 (1993) 299–309.
[41] J. Gustafsson, G. Orädd, M. Almgren, Disintegration of the lecithin lamellar phase by cationic surfactants, Langmuir 13 (1997) 6956–6963.
[42] M. Johnsson, K. Edwards, Interactions between nonionic surfactants and sterically stabilized phosphatidyl choline liposomes, Langmuir 16 (2000) 8632–8642.
[43] M. Johnsson, K. Edwards, Liposomes, disks, and spherical micelles: aggregate structure in mixtures of gel phase phosphatidylcholines and poly(ethylene glycol)-phospholipids, Biophys. J. 85 (2003) 3839–3847.
[44] S. Buchoux, J. Lai-Kee-Him, M. Garnier, P. Tsan, F. Besson, A. Brisson, E.J. Dufourc, Surfactin-triggered small vesicle formation of negatively charged membranes: a novel membrane-lysis mechanism, Biophys. J. 95 (2008) 3840–3849.
[45] M. Deleu, M. Paquot, T. Nylander, Effect of fengycin, a lipopeptide produced by *Bacillus subtilis*, on model biomembranes, Biophys. J. 94 (2008) 2667–2679.
[46] M. Eeman, L. Pegado, Y.F. Dufrene, M. Paquot, M. Deleu, Influence of environmental conditions on the interfacial organization of fengycin, a bioactive lipopeptide produced by *Bacillus subtilis*, J. Colloid Interface Sci. 329 (2009) 253–264.